Inorganic Chemistry

Article

pubs.acs.org/IC

Chemical Modeling of Mixed Occupations and Site Preferences in Anisotropic Crystal Structures: Case of Complex Intermetallic Borides

Volker L. Deringer, Christian Goerens, Marco Esters, Richard Dronskowski, and Boniface P. T. Fokwa*

Institute of Inorganic Chemistry, RWTH Aachen University, Landoltweg 1, D−52056 Aachen, Germany

ABSTRACT: Transition-metal borides show not only promising physical properties but also a rich variety of crystal structures. In this context, quantum-chemical tools can shed light on important facets of the chemistry within such intermetallic borides. Using density-functional theory (DFT), we analyze in detail two phases of significant structural-chemical importance: the recently synthesized $Ti_{1+x}Os_{2-x}RuB_2$ and the isotypical $Ti_{1+x}Os_{3-x}B_2$. Starting from the observation of different Ti/Os occupations in X-ray crystal structure analysis, we assess suitable computational models and rationalize how the interplay of Ti−Ti, Ti−Os, and Os−Os bonds drives the site preferences. Then, we move on to a systematic investigation of the metal−boron bonds which embed the characteristic, trigonal-planar B_4 units within their metallic surroundings. Remarkably, the different Ti−B bonds in $Ti_{1+x}Os_{2-x}RuB_2$ (and also in its ternary derivative) are of vastly different strength, and the strength of these bonds does not correlate with their length. The tools presented in this work are based on simple and insightful chemical arguments together with DFT, and may subsequently be transferred to other intermetallic phases—transition-metal borides and beyond.

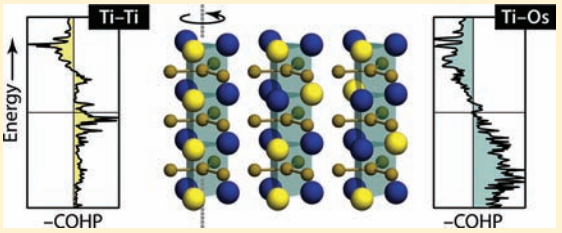

I. INTRODUCTION

Chemical bonding between atoms is a concept so intriguingly straightforward[1] that it survived through centuries and ever-changing paradigms and is still invaluable in the age of modern quantum chemistry. This holds true for solids—three-dimensionally extended bonding networks—just as well.[2,3]

In the latter field, intermetallic solid solutions traditionally provide a rich playground for solid state theorists and experimentalists alike.[4] The growing family of complex intermetallic borides is a prime example, owing to their plethora of fascinating structures and properties.[5] What makes such ternary, quaternary, and quinary[6] borides different from "simple" intermetallics is their mostly berthollide composition, at the same time a chemical challenge and a chance:[5b] it is not uncommon to observe a phase like "$Ti_{(3-x)}Ru_{(5-y)}Ir_yB_{(2+x)}$" in X-ray measurements;[7] furthermore, different atomic species in solid solutions may occupy one crystallographically equivalent position together—take, as a simple example, Fe and Rh atoms in the recently unveiled $FeRh_6B_3$ ferromagnet.[8] The latter issue is widely known as the "coloring problem" in solids.[9−11]

Quantum-theoretical simulations have become a vital complement to X-ray diffraction experiments, and are routinely used to answer numerous questions. To simulate the aforementioned mixed occupations in, say, an intermetallic boride, one must set up the Hamiltonian and thus the quantum-chemical simulation cell with discrete atomic positions that best reflect the mixed occupation. A supercell is currently probably the most common approach: it means going from the X-ray derived simple unit cell (with statistically occupied crystallographic positions) to a doubled, tripled, or larger one by means of a crystallographic transformation. While recent results validate this as a reasonable approximation,[7,8] we will take an alternative approach in this paper. Its first part will describe the systematic construction of simulation cells for a particular intermetallic boride, and a (possibly unorthodox) mnemonic to rationalize such simulation models. However, instead of simply comparing different models energy-wise (which may, in principle, be done by a computer), we will then search for a chemical driving force behind such energy differences—this is what a computer, on its own, *cannot* do. In other words, instead of clinging to larger and larger simulation cells, it is preferable to find a "smart" model through chemical reasoning, which we try to apply in the second part of this paper. In the same spirit, Han and Miller recently studied the magnetocaloric functional material $LaFe_{(13-x)}Si_x$[12] and drew conclusions exactly from such simple concepts: they compared different Si-containing fragments with a semiempirical yet powerful tool—extended Hückel theory (EHT)[13] which is famous for providing insightful orbital symmetry arguments.[14] We will here employ a related but more quantitative approach from density-functional theory (DFT) computations, combining numerically robust data with chemically intuitive concepts[2] as simple as "bond counting".

As subject for this study, we chose the quaternary boride $Ti_{1.6}Os_{1.4}RuB_2$,[15] which we will later call the "parent compound", and its isotypical ternary derivative ($Ti_{1.6}Os_{2.4}B_2$).[16] $Ti_{1.6}Os_{1.4}RuB_2$, first synthetized in 2006 by our own group, is the first known intermetallic boride containing in its crystal structure trigonal-planar B_4 units, a long-missing structural unit until then (as discussed in ref 15, and references therein). The compound with the general

Received: January 4, 2012
Published: May 3, 2012

   dx.doi.org/10.1021/ic300023t | *Inorg. Chem.* 2012, 51, 5677−5685

formula $Ti_{1+x}Os_{2-x}RuB_2$ (x = 0.67 in this work) crystallizes in the hexagonal space group $P\bar{6}2m$ (no. 189) with experimental lattice parameters of a = 8.8554(14) Å and c = 3.0336(7) Å. One unit cell, depicted in Figure 1, contains three formula units.

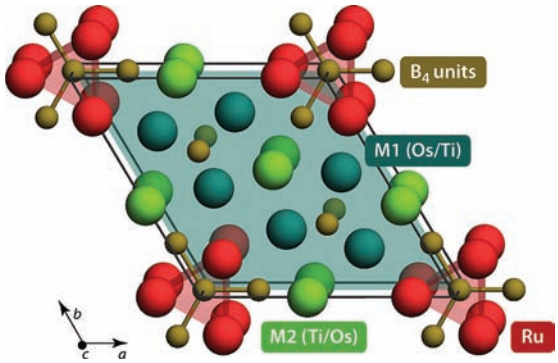

Figure 1. Projection of the crystal structure of $Ti_{1+x}Os_{2-x}RuB_2$ nearly along [001]. Mixed Ti/Os sites are shown in dark green (M1) and light green (M2), Ru atoms are shown in red, and B atoms are shown in brown. Ru_6 prisms surrounding the trigonal-planar B_4 units have been sketched, and the z = 0.5 c plane is indicated in teal. After ref 15.

That being said, another question arises. Intermetallic borides contain several topologically different boron fragments[6] like the B_4 entities here (which are isostructural but not isoelectronic to anions like BO_3^{3-} or BN_3^{6-}), and obviously their surrounding in the crystal plays a key role. To that end, a profound understanding of the metal−boron bonding in such intermetallic compounds is mandatory. So far, the binary TiB_2 and OsB have been investigated[17] using the aforementioned density-functional based bond-analytical tools, but a more comprehensive approach which comprises different metal−boron bonds in more complex borides is yet missing. We will thus analyze how the peculiar trigonal-planar B_4 unit is embedded within the $Ti_{1.6}Os_{1.4}RuB_2$ crystal structure, in seamless extension of the experimental and structural-chemical discussion of 2006.[15] Here, just like for the mixed occupations (which will be tracked back to metal−metal interactions), chemical bonding is the driving force, as we attempt to show in this work.

II. COMPUTATIONAL METHODS

This work is based on ab initio electronic-structure computations of the DFT type. To evaluate different simulation models (i.e., unit cells) energetically, we used the well-established generalized gradient approximation as parametrized by Perdew, Burke, and Ernzerhof (GGA−PBE)[18] together with a plane-wave basis set and the projector augmented-wave (PAW) method[19] as implemented in the Vienna ab initio simulation package (VASP).[20] **k** space was sampled using a Γ-centered Monkhorst−Pack grid[21] (6 × 6 × 6 for "tripled" cells as described in the next section, and the grid was increased appropriately for smaller cells). Cell volumes of all proposed structures were allowed to relax with a convergence criterion of $\Delta E < 10^{-4}$ eV.

To analyze the chemical bonding within the resulting optimized structures in an orbital-pair-resolved way, we performed tight-binding linear muffin-tin orbital (LMTO) computations using the atomic spheres approximation (TB-LMTO-ASA program)[22] and the von Barth−Hedin exchange−correlation potential.[23] Crystal orbital Hamilton populations (COHP)[24] were then calculated from the self-consistent LMTO wave function, and we present them in the conventional manner:[3] we draw −COHP(E) plots so that antibonding interactions lie to the left of the vertical axis, and bonding contributions to the right. The energy zero in −COHP(E) curves has been set to the Fermi level ε_F throughout this work.

III. CHEMICAL BONDING OF THE PARENT COMPOUND, $Ti_{1+x}Os_{2-x}RuB_2$

A. Modeling Mixed Occupations. In our previous publication on the $Ti_{1+x}Os_{2-x}RuB_2$ phase,[15] emphasis was put on the coordination polyhedra and the trigonal-planar B_4 unit. Already then, it was stated that two distinguishable crystallographic positions (designated M1 and M2 in ref 15) bear varying amounts of Ti and Os atoms, and percentage occupations were found. A deeper insight, naturally, could not be accessible from X-ray diffraction alone because specific Ti and Os atoms are not unambiguously resolved against each other. This provides the starting point for our quantum-chemical simulations. Compared to experiment, these allow for a detailed local view and the "singling out" of certain interactions, but in turn every computation needs to be fed with a discrete theoretical model instead of a fractional occupation number. Depending on the system in question, this may be a delicate task: combinatorics easily suggests numerous different models and a theorist needs to choose the most suitable one.[25] Before we can start to analyze the bonds in $Ti_{1+x}Os_{2-x}RuB_2$, a proper model must thus be found.

As reported before,[15] the M2 position has a clear tendency to bear Ti atoms (a 96% Ti content was found from X-ray data). We may safely make the simplifying assumption that M2 is solely occupied by Ti (Ti2), which vastly reduces the complexity of the problem. Furthermore, we set the Ti/Os ratio on the M1 position exactly to 1:2 to achieve a very simple stoichiometric composition (33% Ti + 67% Os, as compared to the experimentally found[15] 31% Ti and 69% Os). These changes result in the chemical formula $Ti_{1.67}Os_{1.33}RuB_2$ (x = 0.67) which is very close to the experimental one (x = 0.6). For the various simulation cells described below, computational optimization yielded cell parameters of a = 8.934 to 8.938 Å and c = 3.060 to 3.062 Å, which is in good agreement with the experimental values of a = 8.8554(14) and c = 3.0336(7) Å,[15] especially in the light of GGA's slight tendency toward "underbinding"[3] and the marginally modified composition. We also note that among different models, the respective bond lengths stay almost unchanged (±0.002 Å) which assures that bonding analyses presented later will be comparable between different models.

So how are the Ti and Os atoms distributed on the M1 (33% Ti + 67% Os) position? The anisotropic structure of $Ti_{1+x}Os_{2-x}RuB_2$ is built up by two different layers alternating along [001], and our first straightforward guess is to triple the unit cell along the c direction (coined the "supercell" approach),[8] filling the M1 positions of one layer with Ti only, and the other M1s in the remaining two layers solely with Os. This goal is achieved by transforming the original cell using an isomorphic group-subgroup relationship. In this case, the 6l Wyckoff position, formerly occupied with the M1 mixture of one-third Ti and two-thirds Os, splits up into a 6k position bearing Ti atoms, and 12l containing Os; the original space group $P\bar{6}2m$ remains unchanged by tripling the cell. The resulting simulation box is displayed in Figure 2. Because of the space group symmetry a further splitting of the osmium 12l site is not possible, which prohibits a mixing of titanium and osmium in identical layers, so generating in-layer Ti−Os contacts is not feasible with this "supercell" approach.

dx.doi.org/10.1021/ic300023t | Inorg. Chem. 2012, 51, 5677−5685

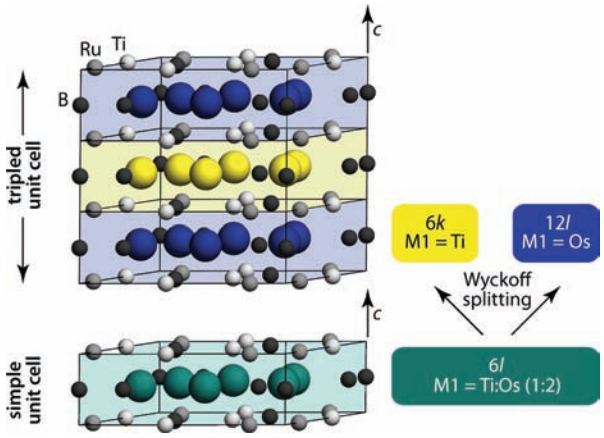

Figure 2. *Left:* Simple unit cell and "layered" model of $Ti_{1+x}Os_{2-x}RuB_2$, obtained by tripling the unit cell in the *c* direction. Os atoms are shown in blue, Ti atoms in yellow; nonrelevant atoms are shown in gray for clarity. *Right:* Resulting splitting of the Wyckoff positions.

Indeed, there is a different route, namely, lowering the symmetry of the unit cell.[25] In the case of our compound, it means breaking the hexagonal symmetry to arrive at a triclinic cell. One unit cell hosts six M1 atoms, and we may conserve the 1:2 stoichiometry by distributing two Ti and four Os atoms on these six M1 positions. Several of the resulting occupations are symmetry-equivalent, but four different arrangements emerge. A simple mnemonic trick helps to designate them: as seen from Figure 3 (top), six M1 atoms (shown in dark green) surround the trigonal-planar B_4 units (brown), forming a distorted hexagon. There must always be two Ti atoms in this hexagon, and their relative positions define the four arrangements; we borrow a notation from organic chemistry, where double substitutions at a hexagonal benzene ring are indicated as "*ortho*", "*meta*" and "*para*".[26] Because the hexagon here is not ideal but distorted, two different possibilities for "*ortho*" configurations exist, namely, connecting the two Ti atoms via a short (2.91 Å) or long (4.26 Å) edge of the hexagon. The four possible arrangements within the hexagon are shown in Figure 3 (middle). After setting up the respective simulation cells, we computed their DFT energies, which are summarized in Table 1. We found major differences between the models, spanning a range of 0.436 eV which corresponds to 14 kJ mol^{-1} simply because of a permutation of "site-equivalent" atoms.[27] The "*ortho-long*" configuration shown in Figure 3 (bottom) turns out to be most stable, closely followed by the "*para*" one which lies only 0.062 eV higher. The "layered" (supercell) model lies in third position and is 0.330 eV higher, but still slightly lower than "*ortho-short*" (+0.371 eV) and "*meta*" (+0.436 eV).

A quick counting of bonds (Table 2) shows that the number of Ti−Ti bonds decreases to zero in the two "stable" configurations; an observation that we will discuss in a moment. Before, let us round out the model and look not only at the M1-containing layers but also at their stacking in the crystal, that is, along the *c* axis. To simulate different possible stacking models, we repeated the unit cell two or three times and rotated the respective cells by 0° ("A"), 120° ("B"), or 240° ("C") around a 3-fold axis in the *c* direction. Our results for four different stacking models are presented in Table 1. Rotating the layers against each other leads to a considerable stabilization and, again, a counting of bonds will be helpful. Given that the distance between the layers is only 3.06 Å, there

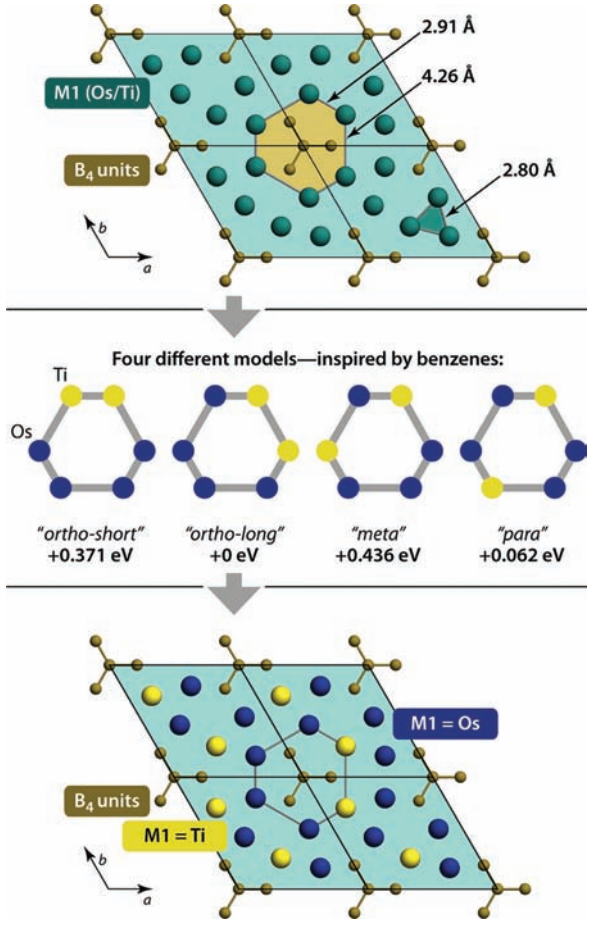

Figure 3. *Top:* 2 × 2 supercell of $Ti_{1.6}Os_{1.4}RuB_2$, viewed along the *c* axis at *z* = 0.5. Structural features are highlighted by shading; note that two slightly different M1−M1 "nearest-neighbor" contacts occur. *Middle:* Schematic representation of the models, and VASP free energies of the corresponding cells, relative to the most stable "*ortho-long*" configuration. *Bottom:* Same view as above, but with distinct M1 occupations as described by the "*ortho-long*" model. Ti atoms are drawn in yellow and Os atoms in blue.

Table 1. Relative Energies (Δ*E*, Per Unit Cell) for Different Structural Models As Discussed in the Text

model (see text)	stacking	Δ*E* (eV)
meta	A	0.436
ortho-short	A	0.371
layered		0.330
para	A	0.062
ortho-long	A	0 (reference)
	AAB−AAB−...	−0.529
	AB−AB−...	−0.742
	ABC−ABC−...	−0.740

are two such Ti−Ti and four Os−Os contacts parallel to the *c* axis if a simple cell is used (i.e., the stacking sequence is A−A−A−...). This is illustrated in Figure 4 (left); for simplicity, we only show the hexagon around the B_4 unit. Upon rotating every third layer (AAB−AAB−...), several Ti−Ti and Os−Os contacts along *c* vanish, as seen from Figure 4 (middle), and the energy is lowered by 0.529 eV per unit cell. Counting the distinct M1−M1 contacts along the *c* axis yields the numbers given in Table 3—as in the previous table but now for interlayer pairs. If, finally, all layers are rotated against each

dx.doi.org/10.1021/ic300023t | *Inorg. Chem.* 2012, 51, 5677−5685

Table 2. Number N of M1−M1 Bonds (d = 2.80−2.91 Å) within the z = 0.5 Layer[a]

	within layer (z = 0.5)		
model	N(Ti−Ti)	N(Ti−Os)	N(Os−Os)
layered	3[b]	0	6[b]
meta	1	4	4
ortho-short	1	4	4
para	0	3	6
ortho-long	0	3	6

[a]Values are given for different models as discussed in the text. M1 is either Ti or Os. [b]Normalized to one unit cell.

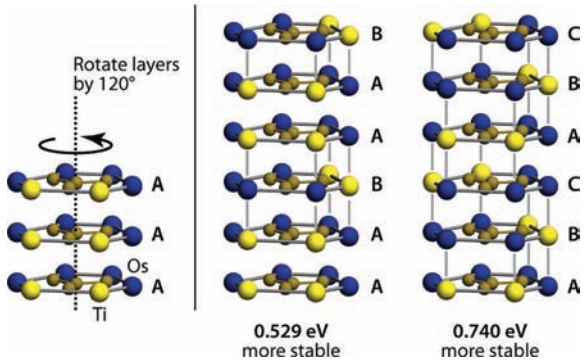

Figure 4. Adding the third dimension: Unit cells of the stable "*ortho-long*" configuration are stacked along the c axis (dashed line) and rotated against each other. Structural fragments (cf. Figure 3) are represented, showing only the B_4-containing layers but with different configurations. *Left:* AAA−AAA−...; *middle*: AAB−AAB−...; *right:* ABC−ABC−... stacking. Ti−Os contacts in c direction are sketched by gray lines. Relative electronic energies are given per simple unit cell.

Table 3. Number N of M1−M1 Bonds along the c Direction (d = 3.06 Å) in Different Stacking Variants of the Most Favorable "ortho-long" Model[a]

	between layers (c direction)		
stacking	N(Ti−Ti)[b]	N(Ti−Os)[b]	N(Os−Os)[b]
A	2	0	4
AAB−AAB−	0.67	2.67	2.67
AB−AB−	0	4	2
ABC−ABC−	0	4	2

[a]As discussed in the text, the same numbers are obtained for the other "benzene" models. M1 is either Ti or Os. [b]Normalized to one unit cell, hence the fractional values.

other (ABC−ABC−..., shown on the right of Figure 4), the interlayer Ti−Ti pairs vanish completely and only two Os−Os ones remain; instead, there are now four Ti−Os pairs along the c axis, and the energy is lowered by 0.740 eV compared to the "simple" cell. We note that an AB−AB−... stacking model is equally powerful as the ABC−ABC−... one (as deduced from their energies given in Table 1, which are equal within numerical deviations, and from the number of Ti−Os contacts given in Table 3), but the AB−AB−... model requires a smaller simulation cell. Finally, all stacking models shown in Figure 4 are energetically superior to the "layered" model (Figure 2). It will now be left to quantum-chemical bonding analysis to investigate why Ti−Os and Os−Os pairs appear to be so obviously favorable over Ti−Ti contacts.

Concluding the discussion of occupation models, the strength of those derived here is obvious: If we are interested in the chemistry within the B_4-containing layer (or in the boron subunit's first coordination sphere), a simple cell is sufficient; the simple "*ortho-long*" cell (which serves as reference in Table 1) is still energetically much preferable to the "layered" model (Figure 2) frequently employed so far. On the other hand, if one seeks to get as close as possible to the experiment, the new model can be improved further by introducing stacking along the c axis, and the overall energy range spanned is an astonishing 1.07 eV, or 34.4 kJ mol^{-1} per formula unit of $Ti_{1+x}Os_{2-x}RuB_2$, just by choosing a more suitable model.

B. Metal−Metal Bonding. As discussed in the previous section, the most stable structures are those where the Ti−Ti bond is nonexistent in the z = 0.5 layer. We seek to investigate this observation by a quantum-chemical bonding analysis: while the most preferable distribution of Ti and Os has been found, it remains to explain which chemical bonding effects drive this preference. To this end, we restrict ourselves to a simple unit cell as discussed before. Within its z = 0.5 layer, there are three kinds of nearest-neighbor interactions: Ti−Ti, Ti−Os, and Os−Os, which have bond lengths of either d(M1−M1) = 2.80 or 2.91 Å. In Figure 5, we show the result of our bonding analysis

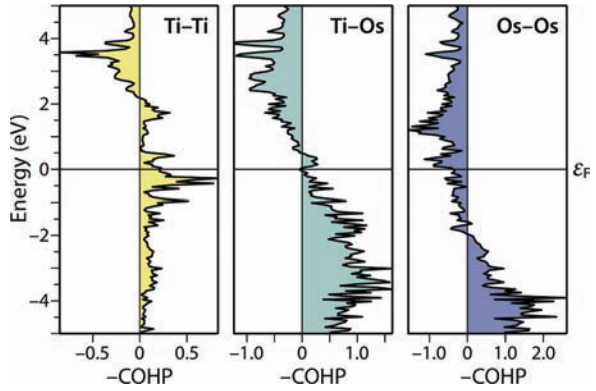

Figure 5. Ti−Ti (*left*), Ti−Os (*middle*), and Os−Os (*right*) crystal orbital Hamilton population (COHP) plots, calculated for $Ti_{1.67}Os_{1.33}RuB_2$ in the "*meta*" configuration (see text).

in the form of COHP curves. These were calculated for the "*meta*" model structure, simply because no Ti−Ti pair is found in the most stable "*ortho-long*" configuration, but it was verified that the results for all models were the same in character.

All three COHP curves show the same general shape near the Fermi level ε_F: the Ti 3d and Os 5d bands, which mostly make up the band structure in this area, split up into a mainly filled bonding area, and an antibonding (negative −COHP values) one, which is mostly empty. While the three kinds of M1−M1 bonds have the same overall character, they differ significantly in detail. For a Ti−Ti pair, the stabilizing bands (indicated by positive −COHP values, Figure 5) are not completely filled and reach up to 2 eV above the Fermi level, indicating a deficit of electrons. Albeit the overall character of the COHP is bonding, the Ti−Ti bond is thus the weakest of the three presented interactions. Moving on to the Ti−Os bond (Figure 5, middle), we can see that nature has nearly optimized this bond: the Fermi level almost coincides with the transition from bonding to antibonding areas; it is obvious why Ti−Os pairs seem advantageous within a layer. Looking, finally, at the Os−Os interactions shown on the right of Figure 5, we notice a

dx.doi.org/10.1021/ic300023t | *Inorg. Chem.* 2012, 51, 5677−5685

further upward shift of the Fermi level (going from a d^2 valence configuration in Ti to a d^6 configuration in Os, the frontier bands are filled up with more electrons)—a large enough shift to push the Fermi level into antibonding areas such that the region from −1.75 eV to the Fermi level actually weakens the Os−Os bond. While below −3.5 eV there are significant bonding interactions that still lead to a strong stabilization in total, we keep in mind that the Os−Os bond appears sensitive to a further upward shift of the Fermi level: Increasing the valence electron count (VEC) will force the valence band edge further into antibonding terrain. In other words, a substitution of osmium by other neighboring 5d transition metals may be advantageous if the VEC is decreased (by Os-substitution for an electron-poorer 5d element) or disadvantageous by increasing the VEC (Os-substitution for an electron-richer 5d element). Indeed, we have recently tried to substitute osmium in $Ti_{1.6}Os_{1.4}RuB_2$ by the one-electron richer iridium, but the parent compound's structure type was not achieved; instead, a phase adopting the $Ti_3Co_5B_2$-type structure was obtained.[6] Further experimental and theoretical work is needed here, without question.

Summarizing, we have provided a chemical argument that explains the clear preference of the "*ortho-long*" and "*para*" models in our computations: Ti and Os atoms on the M1 positions are distributed such that the number of favorable Ti−Os and Os−Os interactions (in a layer) is maximized whereas the most unfavorable Ti−Ti ones are annihilated.

C. Metal−Boron Bonding. The trigonal-planar B_4 unit found in the parent compound is a rare structural fragment. While the boron−boron bonding therein has already been analyzed in ref 15, another question remains: how is this boron unit embedded in the metal framework of the intermetallic boride? In other words, the metal−boron bonding needs to be understood, hoping to unravel the interactions which allow this elusive structural fragment to be stabilized, and we believe the metal−boron interactions play the major role here. Again, a bonding analysis should be helpful, and we present our results for the most stable "*ortho-long*" model.

Figure 6 displays the B_4 unit and its coordination in the crystal: The planar triangle (Figure 6a) is surrounded by metal atoms both "out of plane" (i.e., the metal atom lies in the $z = 0$ plane, Figure 6b,c) and "in plane" (meaning that the metal atoms share the $z = 0.5$ layer with the B_4 unit, Figure 6d). In the former case, we find a trigonal prism of Ru atoms around the central boron atom, and these Ru atoms are both connected to the central B1 atom with a bond length of d(Ru−B1) = 2.18 Å, and to the outer B2 atoms of the triangle with d(Ru−B2) = 2.33 Å, as shown in Figure 6b. Furthermore, there are six Ti−B bonds which connect the outer B2 atoms to the M2 position that (in our model) is occupied exclusively by Ti (Figure 6c); these bonds have a length of d(Ti2−B2) = 2.39 Å. As for "in plane" interactions, the B_4 unit is surrounded by the distorted hexagon we discussed before; it is shown in Figure 6d for the most stable "*ortho-long*" configuration, and the bond lengths are d(Ti1−B2) = d(Os−B2) = 2.36 Å. Clearly, the B_4 unit has a most diverse environment, and we will now investigate it step by step.

As before, we performed COHP analyses for the different bonds. Figure 7 shows the resulting curves, namely, for "out of plane" Ti2−B and Ru−B bonds (top) and those to the hexagon (Ti1−B and Os−B, bottom). We will start our discussion with the curves' most striking feature, namely, the fact that Ti2−B bonds appear much stronger than their Ti1−B counterparts

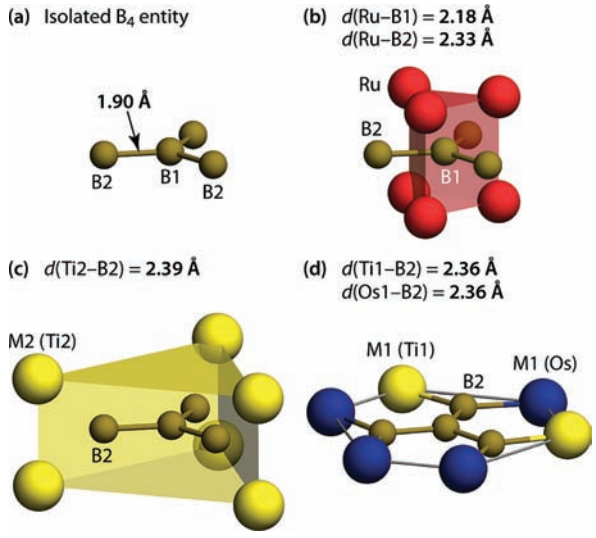

Figure 6. Coordination geometries around a trigonal-planar B_4 unit (a): six Ru atoms (b), out-of-plane Ti atoms (c), and the Ti/Os hexagon discussed before (d).

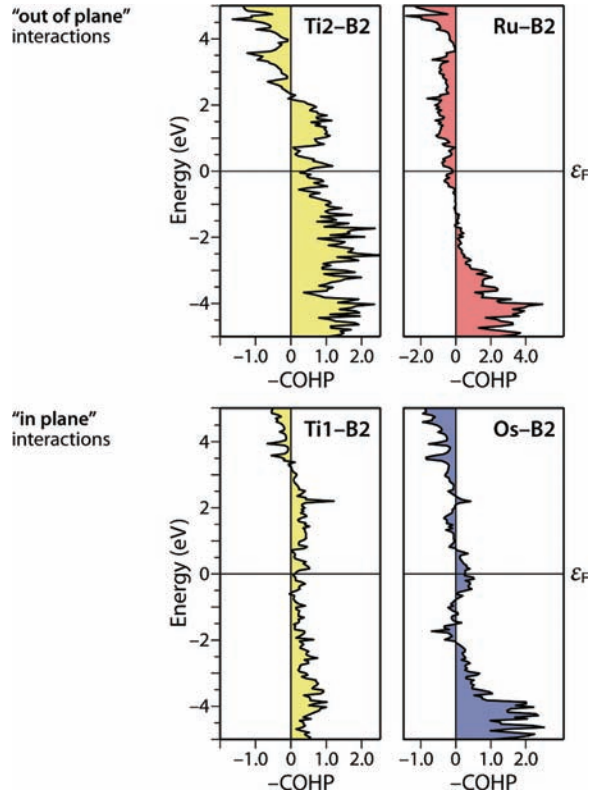

Figure 7. Metal−boron COHPs, corresponding to the bonds specified in Table 4. All bonds refer to the B2 atom on the corner of the trigonal-planar unit; the Ru−B1 COHP curve has been left out for brevity.

because the numerical COHP values in the valence bands are considerably higher. Indeed, an energy integration up to the Fermi level (−ICOHP) reveals stabilizing values of 2.09 eV (Ti2) and 1.66 eV (Ti1) that parallel this observation in a more quantitative way. Looking back at the crystal structure, this is especially puzzling since the Ti1−B bonds, albeit weaker, are shorter than the 26% stronger Ti2−B bonds. A simple bond length−bond strength ansatz is thus not sufficient in this case.

dx.doi.org/10.1021/ic300023t | Inorg. Chem. 2012, 51, 5677−5685

In return, we assume that this finding may partly explain the vastly different occupations on the M1 and M2 positions by titanium and osmium: Ti−B bonds are considerably stronger when Ti sits on the M2 (96% Ti + 4% Os) position and this may be what drives the experimentally observed site preference; the osmium atoms, meanwhile, mainly occupy the M1 (33% Ti + 67% Os) position which would be less favorable for the Ti−B bonding. In the latter case, the COHP curve for the Os−B bond (Figure 7, bottom right) shows strong stabilizing interactions (−ICOHP = 2.18 eV),[28] most pronounced in the area up to −3.5 eV. In the bands closest to the Fermi level, that is, from −3.5 eV to around +3 eV, no definitive assessment of the bonding characteristic is possible (the integral over this area is close to zero), but the lower-lying areas strongly stabilize the Os−B bond in this structure.

Finally, there are Ru−B bonds to consider. As Figure 6b shows, ruthenium atoms form a trigonal prism which encases the B_4 entity, and two different kinds of bonds emerge: there are six nearest-neighbor contacts between Ru and the central B1 atom (d = 2.18 Å), and the trigonal prism is thrice overcapped (by B2 atoms) which results in another twelve ruthenium−boron bonds (d = 2.33 Å), namely, those to the outer B2 atoms. A COHP analysis characterizes these Ru−B bonds as very strong, especially those to the inner boron atom with −ICOHP(Ru−B1) = 2.48 eV per bond; the bonds outside the trigonal prism are firm as well, and energy integration gives −ICOHP(Ru−B2) = 2.00 eV per bond. Because one unit cell contains 6 of the former bonds and 12 of the latter, they also offer the largest total contribution to the "embedding" of the B_4 unit in the metal framework. A detailed look at the shape of the ruthenium−boron COHP curve (Figure 7, top right), however, indicates weakly antibonding states around −0.5 eV and above such that the Fermi level lies in a destabilizing area. This is the case for the Ru−B2 COHP shown here, as well as for the comparable Ru−B1 COHP curve which we omitted for brevity. Such an observation, again, is crucial when dealing with substitutions that change the valence electron count (VEC), which is frequently done in experiments.[6] We conclude our analysis of the B_4 unit's bonding by summing up all its nearest-neighbor interactions present in one unit cell in Table 4. It is found that 18 Ru−B bonds make up the majority (61%) of all computed metal−boron contributions to the ICOHP (which, in turn, are additive contributions to the band-structure energy[24]). The second largest part (25%, or 15.84 eV) stems from a total of 8 Ti−B bonds which are considerably stronger if the Ti atoms lie outside the B_4-containing layer. Finally, there are 4 Os−B bonds per cell which account for 8.72 eV (14%) of the total metal−boron ICOHP contributions listed.

Table 4. Boron−Metal Bonds around the B_4 Unit: Bond Lengths *d*, Number of Bonds Per Unit Cell *N*, and −ICOHP Values Per Bond and Per Unit Cell

bond	*d* (Å)	*N*	−ICOHP (eV) per bond	−ICOHP (eV) per cell
Ti1−B2	2.359	2×	1.657	3.314
Ti2−B2	2.393	6×	2.088	12.526
Os−B2	2.359	4×	2.180	8.721
Ru−B1	2.179	6×	2.482	14.892
Ru−B2	2.327	12×	2.002	24.024

IV. EXEMPLARY APPLICATION: THE TERNARY $Ti_{1+x}Os_{3-x}B_2$ PHASE

Following the synthesis of $Ti_{1+x}Os_{2-x}RuB_2$, the experimentalists' next step was to try and create more phases which would contain the trigonal-planar B_4 moiety. One of the simplest compositions they imagined is an isotypical ternary phase, where Os would formally take the place of Ru atoms to arrive at the general formula $Ti_{1+x}Os_{3-x}B_2$ (x = 0.6). Indeed, the compound was successfully synthesized two years later from the elements by arc-melting.[16] Intuitively, one might assume that Os will replace Ru on the M3 position, because both have the same number of valence electrons, and also their atomic radii r_A are quite similar, namely, r_A(Ru) = 1.315 Å and r_A(Os) = 1.328 Å.[29] So will Os take Ru's place? We will use a notation which directly expresses the site occupations and this way, the parent compound $Ti_{1.67}Os_{1.33}RuB_2$ is written as

$$[Ti_{0.67}Os_{1.33}]^{M1}[Ti]^{M2}[Ru]^{M3}B_2 \quad (1)$$

while the above-mentioned hypothetical substitution can be expressed by the "reaction"

$$[Ti_{0.67}Os_{1.33}]^{M1}[Ti]^{M2}[Ru]^{M3}B_2 + Os \rightarrow [Ti_{0.67}Os_{1.33}]^{M1}[Ti]^{M2}[Os]^{M3}B_2 + Ru \quad (2)$$

leaving the rest of the crystal structure (most importantly, the mixed occupation on M1) untouched and arriving at the formula $Ti_{1.67}Os_{2.33}B_2$—slightly simplified again in comparison to experiment because we have x = 0.67, as discussed for the parent compound above.

The reality is, however, very different from our hypothesis: X-ray diffraction shows with certainty[16] that the Ti/Os mixed occupation occurs on the M3 position exclusively. M2 contains Ti in the experimentally refined ternary structure, as well, and M1 (in the z = 0.5 layer) bears only Os atoms. As a further simplification, it is noted that split M1 (Os) positions were observed in the experiment,[16] but we neglect this circumstance because it does not influence the comparison between different chemical bonds we perform here. The unit cell of this ternary phase is shown in Figure 8 (bottom).

To corroborate these experimental findings, we may approximate the enthalpy of "reaction" (eq 2) as a DFT free-energy difference (ΔE_R) between product and educt sides (neglecting minute thermal effects for now) which gave ΔE_R = +39.7 kJ mol^{-1}; in other words, the hypothetical substitution reaction is predicted to be endothermic, hence favoring the quaternary phase (educt). In the next step, we simulated a reaction similar to eq 2 but leading to the experimentally verified structure, and in this case we have

$$[Ti_{0.67}Os_{1.33}]^{M1}[Ti]^{M2}[Ru]^{M3}B_2 + Os \rightarrow [Os]^{M1}[Ti]^{M2}[Ti_{0.67}Os_{1.33}]^{M3}B_2 + Ru(\Delta E_R = -99.3\,\text{kJ mol}^{-1}) \quad (3)$$

$$[Ti_{0.67}Os_{1.33}]^{M1}[Ti]^{M2}[Ru]^{M3}B_2 + Os \rightarrow [Os]^{M1}[Ti_{0.67}Os_{1.33}]^{M2}[Ti]^{M3}B_2 + Ru(\Delta E_R = -52.1\,\text{kJ mol}^{-1}) \quad (4)$$

which is predicted to be exothermic (ΔE_R < 0). To round out the picture, we finally simulated another site preference by placing the mixed occupation at the M2 position (see Figure 8,

dx.doi.org/10.1021/ic300023t | Inorg. Chem. 2012, 51, 5677−5685

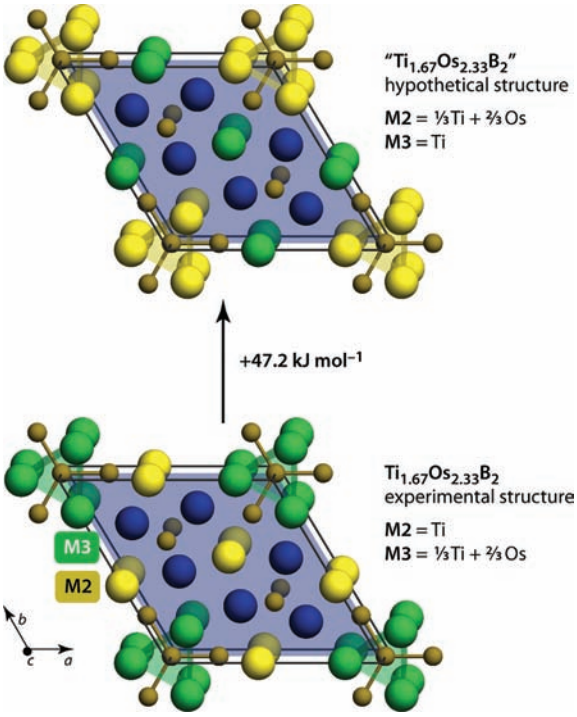

Figure 8. Crystal structure of $Ti_{1.67}Os_{2.33}B_2$ projected nearly along [001]. Ti atoms are shown in yellow, Os atoms in blue, and Ti/Os mixed occupations in green. Besides the experimentally observed structure (bottom), a hypothetical alternative is shown which lies 47.2 kJ mol^{-1} higher in terms of electronic energy.

top); in turn, M3 must change to a purely Ti-bearing one in this case, leading to the following "reaction":

Although eq 4 is also predicted to be exothermic ($\Delta E_R < 0$), it is energetically unfavorable by 47.2 kJ mol^{-1} if compared to the experimentally verified "reaction" (eq 3). Obviously, option eq 2 is energetically far off (endothermic reaction), and we will try to discriminate only between eq 3 and eq 4; in other words, we seek an explanation for the unambiguous site preference observed in the experiment. As laid out in the preceding section, an atom-pair resolved view is established through an ICOHP analysis.

We summarize the results for all bonds between M2/M3 and the boron atoms of the B_4 unit in Table 5. We will first discuss the metal−boron bonding in the experimentally obtained structure (left part of Table 5) and then move on to the hypothetical phase obtained via eq 4, in the right part of Table 5.

Not surprisingly, the trigonal M3 prism in $Ti_{1.67}Os_{2.33}B_2$ makes the largest ICOHP contributions to the B_4 unit which it encases, like in the parent compound. In particular, the M3−B1 bonds (i.e., those involving the central B atom) are much stronger than their M3−B2 counterparts (between the M3 prism and the outer B atoms). Compared to the quaternary parent compound where the M3 prism contains Ru atoms (shown in Figure 6b), the trigonal M3 prism is here occupied by Os/Ti, and Os3 binds much stronger than Ti3 to the central B1 atom (−ICOHP difference 0.84 eV per bond) and to the outer B2 atoms (difference 0.53 eV per bond) as well. Summing up these contributions, they make up 35.92 eV, equaling 74% of the metal−boron ICOHPs listed in Table 5. The "outer" prism contains six M2−B2 bonds per unit cell, and like in the parent compound, there is only Ti on the M2

Table 5. Metal−Boron Bonds Surrounding the B_4 Unit in $Ti_{1.67}Os_{2.33}B_2$ (Fig. 8): Number of Bonds in the Unit Cell *N* and −ICOHP Values Per Bond and Per Unit Cell[a]

	$Ti_{1.67}Os_{2.33}B_2$ (stable phase)			"$Ti_{1.67}Os_{2.33}B_2$" (hypothetical model)		
	mixed occupation on M3			mixed occupation on M2		
bond	*N*	−ICOHP (eV) per bond	−ICOHP (eV) per cell	*N*	−ICOHP (eV) per bond	−ICOHP (eV) per cell
Ti3−B1	4×	2.056	8.224	6×	2.056	12.336
Os3−B1	2×	2.898	5.796	*b*	*b*	*b*
Ti3−B2	8×	1.649	13.192	12×	1.607	19.284
Os3−B2	4×	2.177	8.708	*b*	*b*	*b*
Ti2−B2	6×	2.061	12.366	4×	2.118	8.472
Os2−B2	*b*	*b*	*b*	2×	2.644	5.288
sum			**48.286**			**45.380**

[a]Values are given both for the stable, the X-ray derived structure (left), and the hypothetical one having a different mixed occupation (right). [b]In the respective model, there are no mixed occupations on this position. There are thus no Os−B nearest-neighbor bonds in this case, but only Ti−B ones.

position (see Figure 6c). The strength of these bonds, if one takes the −ICOHP(Ti2−B2) values as a measure, is 2.06 eV, while for similar bonds in the parent compound, −ICOHP-(Ti2−B2) = 2.09 eV was found (Table 4). Given the close relationship between both phases, those numerical values are to a good extent comparable (albeit not entirely on equal footing because different underlying band-structure energies are dissected into different −ICOHP values).[24]

Returning to the initial question, what happens if the Ti/Os mixed occupation is "forced" onto the M2 position—and, more importantly, why is this hypothetical model (Figure 8, top) ruled out both by our computations and by experiment? Analyzing the −ICOHP values in Table 5 may lead to an answer. Albeit the number *N* of specific bonds within the unit cell changes, their total number stays the same; as ICOHP are additive contributions to the band-structure term,[24] they may be summed up and compared in convenient ways, in this case, for the M2 and M3 prisms. This sum is much higher for the experimental model (see Table 5). The total −ICOHP of M3−B bonds is 31.63 eV in the hypothetical structure compared to 35.92 eV in the experimental one; the inner M3 prism binds less strongly to the trigonal-planar B_4 unit, because especially the Ti3−B2 bonds are weak (here, −ICOHP = 1.61 eV), and the strong Os3−B2 bonds observed in the "experimental" $Ti_{1.67}Os_{2.33}B_2$ are absent here. In return, bonds between the outer M2 prism and the B_4 unit get stronger in the hypothetical structure (30% versus 26% contribution), but the overall effect is destabilizing because, in a very simplified language, going from the experimental to the hypothetical structure means trading "strong" Ti2−B bonds for "weak" Ti3−B ones. The decrease in ICOHP values is reflected in the electronic energy differences; there is however no one-to-one relationship between both (even if both computations would be performed with the same program), as needs to be mentioned as another word of caution.

Finally, now that computational evidence for the mixed occupation on M3 has been presented in accordance with experimental work,[16] we will round out the picture by comparing different models for mixed occupations along the *c* axis. We will not reiterate the discussion of the previous

dx.doi.org/10.1021/ic300023t | Inorg. Chem. 2012, 51, 5677−5685

section but directly present results for three different stacking models in Figure 9. In order of increasing stability, the number

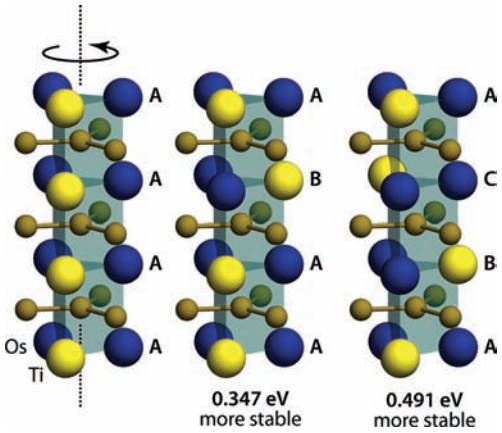

Figure 9. Different stacking models along the *c* direction as in Figure 4, but for the trigonal Ti/Os prisms around the B4 units in $Ti_{1.67}Os_{2.33}B_2$. Electronic energies relative to the least stable "AAA–AAA– ..." configuration are given per simple unit cell.

of Ti–Ti contacts along the *c* axis (normalized to one unit cell like in Table 3) decreases from 1 to 0.33 to zero; the number of Os–Os bonds goes as 2–1.33–1, and the number of Ti–Os contacts increases from zero (AAA–AAA–...) to 1.33 (AAB–AAB–...), and finally to 2 in the most stable ABC–ABC–... configuration. The total electronic energy gain by introducing an "optimized" stacking model along *c* is 0.491 eV per simple unit cell, as compared to 0.740 eV for the parent compound—there, a larger number of metal–metal contacts was involved and thus the total gain was somewhat higher. Summarizing, the quantum-chemical modeling for the parent compound could be transferred to the ternary phase, and an analysis of the metal–boron bonding provided chemically insightful arguments in this case, too.

Beyond that, we expect that the routes presented here may be further transferrable to other solid-state structures; here are two examples. Among B_n fragments, planar boron rings or "wheels" have been investigated by theory and gas-phase experiments,[30] and were found in a few organometallic compounds[31] and, very recently, in a solid state phase.[32] To explore how, in the latter case, the planar B_6 ring is embedded within its metal surrounding will again raise the question of metal–boron interactions; a theoretical analysis of different metallic surroundings could lead, eventually, to new synthetic targets. Beyond borides, polar intermetallics (e.g., substituted Zintl phases) frequently show mixed occupations, often within anisotropic crystal structures;[33] many of these phases have been studied successfully with combined experimental and DFT-based bond-analytical approaches.[25] Recipes like "counting bonds" both within and between the layers, as well as a look at the metal–metal interactions on mixed sites, may provide additional chemical insight in many such cases.

V. CONCLUSIONS

In this work, we have looked at complex intermetallic borides from a quantum chemical perspective, specifically, at the parent compound $Ti_{1+x}Os_{2-x}RuB_2$ as well as an isotypic ternary derivative, $Ti_{1+x}Os_{3-x}B_2$, which both contain a hitherto unprecedented, trigonal-planar B_4 unit.

In the first part, we assessed various computational models to simulate the mixed occupations in the aforementioned solid-state phase. Different simulation cells for the same compound lie apart, energy-wise, as much as 34.4 kJ mol^{-1}, which underlines the importance of a careful choice of chemical model whenever one is dealing with mixed occupations. Moreover, instead of simply listing energies, these effects can be understood as the interplay of chemical bonds which are here revealed by the COHP technique.

We also analyzed how the trigonal-planar B_4 unit is bound within the intermetallic framework. The main contribution stems from Ru–B bonds, and a numerical analysis was done by integrating the $-COHP(E)$ curves up to the Fermi level as in previous studies by others and our own group. Furthermore, it was revealed that two strongly different kinds of Ti–B bonds occur in the intermetallic boride, which is especially puzzling since the weaker bond is somewhat shorter, in contrast to a chemist's intuitive guess.

Finally, we showed exemplarily how the approach may be adapted to a different boride phase, for which the results are in sound agreement with the trends found for the parent compound. The site preferences in $Ti_{1+x}Os_{3-x}B_2$ could be traced back to chemical bonding interactions once more.

AUTHOR INFORMATION

Corresponding Author

*E-mail: boniface.fokwa@ac.rwth-aachen.de.

Notes

The authors declare no competing financial interest.

ACKNOWLEDGMENTS

We thank the German National Academic Foundation (scholarship to V.L.D.), the National Research Fund, Luxembourg (scholarship to C.G.), and the Deutsche Forschungsgemeinschaft (Heisenberg fellowship to B.P.T.F., as well as generous funding).

REFERENCES

(1) (a) Lewis, G. N. *J. Am. Chem. Soc.* **1916**, *38*, 762–785. (b) Pauling, L. *The Nature of the Chemical Bond*; Cambridge University Press: Cambridge, 1960. (c) Hund, F. *Angew. Chem., Int. Ed. Engl.* **1977**, *16*, 87–91. (d) Burdett, J. K. *Chemical Bonds: A Dialog*; VCH: Weinheim, Germany, 1997.

(2) (a) Hoffmann, R. *Angew. Chem., Int. Ed. Engl.* **1987**, *26*, 846–878. (b) Hoffmann, R. *Solids and Surfaces. A Chemist's View of Bonding in Extended Structures*; VCH: Weinheim, Germany, 1988.

(3) Dronskowski, R. *Computational Chemistry of Solid-State Materials*; Wiley-VCH: Weinheim, Germany, 2005.

(4) Miller, G. J. *Chem. Soc. Rev.* **2006**, *35*, 799–813 , and references therein.

(5) (a) Korsukova, M. M.; Gurin, V. N.; Otani, Sh.; Ishizawa, Y. *Solid State Commun.* **1996**, *99*, 215–219. (b) Dronskowski, R.; Korczak, K.; Lueken, H.; Jung, W. *Angew. Chem., Int. Ed.* **2002**, *41*, 2528–2532. (c) Togano, K.; Badica, P.; Nakamori, Y.; Orimo, S.; Takeya, H.; Hirata, K. *Phys. Rev. Lett.* **2004**, *93*, 247004. (d) Samolyuk, G. D.; Fokwa, B. P. T.; Dronskowski, R.; Miller, G. J. *Phys. Rev. B* **2007**, *76*, 094404. (e) Weinberger, M. B.; Levine, J. B.; Chung, H.-Y.; Cumberland, R. W.; Rasool, H. I.; Yang, J.-M.; Kaner, R. B.; Tolbert, S. H. *Chem. Mater.* **2009**, *21*, 1915–1921.

(6) For reviews, see: (a) Bauer, F.; Halet, J.-F.; Saillard, J.-Y. *Coord. Chem. Rev.* **1998**, *178–180*, 723–753. (b) Mori, T. Higher Borides. In *Handbook on the Physics and Chemistry of Rare Earths*; Gschneidner Jr., K. A., Bünzli, J.-C., Pecharsky, V. K., Eds.; North-Holland: Amsterdam, The Netherlands, 2007; Vol. *38*, pp 105–173. (c) Fokwa, B. P. T. *Eur. J. Inorg. Chem.* **2010**, 3075–3092.

(7) Fokwa, B. P. T.; Hermus, M. *Inorg. Chem.* **2011**, *50*, 3332−3341.
(8) Misse, P. R. N.; Gilleßen, M.; Fokwa, B. P. T. *Inorg. Chem.* **2011**, *50*, 10303−10309.
(9) Burdett, J. K.; Lee, S.; McLarnan, T. J. *J. Am. Chem. Soc.* **1985**, *107*, 3083−3089.
(10) (a) Miller, G. J. *Eur. J. Inorg. Chem.* **1998**, 523−536. (b) Miller, G. J. *Z. Anorg. Allg. Chem.* **2006**, *632*, 2078.
(11) Rocquefelte, X.; Boulfelfel, S. E.; Yahia, M. B.; Bauer, J.; Saillard, J.-Y.; Halet, J.-F. *Angew. Chem., Int. Ed.* **2005**, *44*, 7542−7545.
(12) Han, M.-K.; Miller, G. J. *Inorg. Chem.* **2008**, *47*, 515−528.
(13) (a) Hoffmann, R. *J. Chem. Phys.* **1963**, *39*, 1397−1412. (b) Hoffmann, R. *J. Chem. Phys.* **1964**, *40*, 2474−2480. (c) Hoffmann, R. *J. Chem. Phys.* **1964**, *40*, 2745.
(14) (a) Burdett, J. K.; Canadell, E.; Hughbanks, T. *J. Am. Chem. Soc.* **1986**, *108*, 3971−3976. (b) Whangbo, M.-H.; Hoffmann, R. *J. Am. Chem. Soc.* **1987**, *100*, 6093−6098. (c) Stability trends for Ta_3B_4-type transition-metal borides were successfully explored based, again, on extended Hückel theory and the COOP technique: Minyaev, R. M.; Hoffmann, R. *Chem. Mater.* **1991**, *3*, 547−557.
(15) Fokwa, B. P. T.; von Appen, J.; Dronskowski, R. *Chem. Commun.* **2006**, 4419−4421.
(16) Fokwa, B. P. T.; Dronskowski, R. *Z. Anorg. Allg. Chem.* **2008**, *634*, 1955−1960.
(17) Fokwa, B. P. T.; Misse, P. R. N.; Gilleßen, M.; Dronskowski, R. *J. Alloys Compd.* **2010**, *489*, 339−342.
(18) Perdew, J. P.; Burke, K.; Ernzerhof, M. *Phys. Rev. Lett.* **1996**, *77*, 3865−3868.
(19) Blöchl, P. E. *Phys. Rev. B* **1994**, *50*, 17953−17979.
(20) (a) Kresse, G.; Hafner, J. *Phys. Rev. B* **1993**, *47*, 558−561. (b) Kresse, G.; Furthmüller, F. *Comput. Mater. Sci.* **1996**, *6*, 15−50. (c) Kresse, G.; Joubert, D. *Phys. Rev. B* **1999**, *59*, 1758−1775.
(21) Monkhorst, H. J.; Pack, J. D. *Phys Rev. B* **1976**, *13*, 5188−5192.
(22) (a) Andersen, O. K. *Phys. Rev. B* **1975**, *12*, 3060−3083. (b) Andersen, O. K.; Jepsen, O. *Phys. Rev. Lett.* **1984**, *53*, 2571−2574.
(23) von Barth, U.; Hedin, L. *J. Phys. C: Solid State Phys.* **1972**, *5*, 1629−1642.
(24) Dronskowski, R.; Blöchl, P. E. *J. Phys. Chem.* **1993**, *97*, 8617−8624.
(25) (a) You, T.-S.; Miller, G. J. *Inorg. Chem.* **2009**, *48*, 6391−6401. (b) Xia, S.-Q.; Myers, C.; Bobev, S. *Eur. J. Inorg. Chem.* **2008**, 4262. (c) Saparov, B.; Xia, S.-Q.; Bobev, S. *Inorg. Chem.* **2008**, *47*, 11237−11244. (d) You, T.-S.; Tobash, P. H.; Bobev, S. *Inorg. Chem.* **2010**, *49*, 1773−1783.
(26) International Union of Pure and Applied Chemistry. *Nomenclature of Organic Chemistry, Sections A, B, C, D, E, F, and H*; Pergamon Press: Oxford, U.K., 1979.
(27) Recall that there are three formula units per unit cell, and thus the eV value per cell must be divided by three upon conversion to kJ per *mole*.
(28) In a previous work on OsB,[17] we touched upon the Os−B bond in the title compound and found a numerically different ICOHP value. This is not surprising because the computations in ref 17 were performed using a different exchange−correlation approximation technique and functional (Volko−Wilk−Nusair). The results presented here are internally consistent.
(29) Pauling, L.; Kamb, B. *Proc. Natl. Acad. Sci. U.S.A.* **1986**, *83*, 3569−3571.
(30) (a) Alexandrova, A. N.; Boldyrev, A. I.; Zhai, H.-J.; Wang, L.-S. *Coord. Chem. Rev.* **2006**, *250*, 2811−2866. (b) Romanescu, C.; Galeev, T. R.; Li, W.-L.; Boldyrev, A. I.; Wang, L.-S. *Angew. Chem., Int. Ed.* **2011**, *50*, 9334−9337. (c) Li, W.-L.; Romanescu, C.; Galeev, T. R.; Piazza, Z. A.; Boldyrev, A. I.; Wang, L.-S. *J. Am. Chem. Soc.* **2012**, *134*, 165−168.
(31) A very recent example is found in Schulenberg, N.; Wadepohl, H.; Himmel, H.-J. *Angew. Chem., Int. Ed.* **2011**, *50*, 10444−10447.
(32) Fokwa, B. P. T.; Hermus, M. *Angew. Chem., Int. Ed.* **2012**, *51*, 1702−1705.
(33) (a) A practical example where mixed occupations in a layered structure enhance material properties is the use of Zintl phases as thermoelectrics; see, for example, Gascoin, F.; Ottensmann, S.; Stark, D.; Haïle, S. M.; Snyder, G. J. *Adv. Funct. Mater.* **2005**, *15*, 1860−1864. (b) A review is given by Kauzlarich, S. M.; Brown, S. R.; Snyder, G. J. *Dalton Trans.* **2007**, 2099−2107.